Pattern Recognition Letters 32 (2011) 1503–1510

Contents lists available at ScienceDirect

Pattern Recognition Letters

journal homepage: www.elsevier.com/locate/patrec

A novel Hough transform method for line detection by enhancing accumulator array

Junhong Ji *, Guodong Chen, Lining Sun

State Key Laboratory of Robotics and System, Harbin Institute of Technology, No.2, Yikuang Str., Harbin 150080, PR China

ARTICLE INFO

Article history:
Received 26 March 2009
Available online 18 April 2011
Communicated by R. Davies

Keywords:
Hough transform
Image processing
Peak detectors
Pattern recognition
Feature extraction

ABSTRACT

In this paper, an improved Hough transform (HT) method is proposed to robustly detect line segments in images with complicated backgrounds. The work focuses on detecting line segments of distinct lengths, totally independent of prior knowledge of the original image. Based on the characteristics of accumulation distribution obtained by conventional HT, a local operator is implemented to enhance the difference between the accumulation peaks caused by line segments and noise. Through analysis of the effect of the operator, a global threshold is obtained in the histogram of the enhanced accumulator to detect peaks. Experimental results are provided to demonstrate the efficiency and robustness of the proposed method.

1. Introduction

Straight lines are frequently adopted as a geometric element in high level image processing or object detection. Detecting line segments is a fundamental issue in image processing. Some methods have been proposed, e.g. chain code (Lu et al., 2005), hidden Markov model based methods (Zheng et al., 2005), knowledge based methods (Li et al., 2008), PCA (Liu et al., 2003), Bayesian methods (Bonci et al., 2005), wavelet (Chien and Li, 1997), Ridgelet transform method (Hou et al., 2003) and subspace (Aghajan and Kailath, 1995).

Compared with other methods, Hough transform (HT) is recognized as a powerful tool to extract parameterized curves (Hough, 1962). Its major advantages include dealing with noise, degradation and partial disconnection and ease of realization. Many improved HT methods have been proposed to extract straight lines, circles, ellipses and natural shapes. Usually, a HT method consists of the following phases: voting, peaks localization, determining the actual parameters and verification.

The voting process has been well investigated and various voting patterns have been adopted to accelerate the accumulation and/or highlight the peaks, e.g. probabilistic HT (Kiryati et al., 1991; Shaked et al., 1996), randomized HT (Xu et al., 1990; Xu and Oja, 1993), sampling HT (Ser and Siu, 1992), heteroscedastic HT (Kiryati and Bruckstein, 2000), progressive probabilistic HT (Matas et al., 2000) etc. A smooth kernel and iterative optimization algorithm is proposed to determine the line parameters with better accuracy (Palmer et al., 1997).

Taxonomically, there are two major peak localization methods: local and global. The former takes the maxima in each $N \times N$ neighborhood over the whole accumulator array, where the choice of N is a critical task. For the latter, choosing the global threshold is also a critical task. For many methods, some prior knowledge is needed to determine the threshold.

Some work focuses on determining the line's complete geometric description through analysis of the spread of votes around a peak in the accumulator array (Atiquzzaman and Akhtar, 1995) or using an intuitive weighting scheme based on likelihood ratio test statistics (Yang et al., 1997). However, before extracting the complete information, thresholds still need to be specified by prior knowledge to determine whether there are some lines.

During voting, the accumulator array can be extended to provide more information. Utilizing both HT parameters and image spaces, a boundary recorder is proposed to improve efficiency and to detect line thickness (Song and Lyu, 2005). The effect is demonstrated with large-size engineering drawings of degraded quality.

Background information is also considered to improve detection (Yang et al., 1997; Cha et al., 2006; Soffer and Kiryati, 1998). Since constructing a universal model of all backgrounds is extremely difficult, some assumptions e.g. a Gaussian or a Poisson distribution are adopted. The results show the improvements of noisy images.

The voting patterns around peaks in the accumulator array have also been analyzed to remove the contribution of background, including noises, artifacts and natural objects (Furukawa and Shinagawa, 2003). A 'butterfly' pattern is adopted and distinguished from the background by evaluating the cross-correlation.

* Corresponding author.
E-mail addresses: junhong.ji@hit.edu.cn (J. Ji), guodongxyz@163.com (G. Chen), lnsun@hit.edu.cn (L. Sun).

0167-8655/$ - see front matter © 2011 Elsevier B.V. All rights reserved.
doi:10.1016/j.patrec.2011.04.011

A similar model is also adopted in Leavers and Boyce (1987)) using the Radon transform and detection is performed via a convolution mask. Parameters still have to be specified and also have obvious influence on the total performance.

A novel method is proposed to detect line segments in images with complicated backgrounds. The objective is to robustly detect line segments of distinct length based on as little prior knowledge as possible. The butterfly pattern is also considered. The major difference between our method and above mentioned methods is as follows. Instead of identifying the total butterfly, its geometric characteristics are considered; then a local operator is implemented to enhance the butterfly's peak. As a consequence, it is more feasible to determine a global threshold to distinguish lines with noise. Since no information with respect to the butterfly is required, there is no demand of prior knowledge about the original image.

The rest of this article is organized as follows. Next section describes the local enhancing operator, section 3 explains how to determine the global threshold to locate peaks, the experimental results are provided in section 4, and finally, the conclusion is given.

2. The local operator enhancing ideal peaks

2.1. The accumulator array dimension

A line's equation is expressed by Duda and Hart (1972):

$$\rho = x\cos\theta + y\sin\theta. \tag{1}$$

Essentially, a line segment in a digital image is a set of pixels. According to Eq. (1), each pixel is projected to a sine curve in the parameter space. In rest of this article, a 'point' in the image and the accumulator is called a pixel and a unit, respectively. The image and accumulator frame are defined in Duda and Hart (1972). Depending on the number of rows and columns in the original image, n_r and n_c, the parameters ρ and θ vary inside ranges of $[-n_r, \sqrt{n_r^2+n_c^2})$ and $[0,\pi)$, respectively.

To distinguish radial and angular differences caused by one pixel, the accumulator resolution is chosen as $d_\rho = 1$ and $d_\theta = \arctan\left(\frac{1}{max(n_r,n_c)}\right)$, then the accumulator's size is determined by the original image's size. For simplicity, they are set as integer powers of 2, the actual dimension are:

$$n_\rho = 2^{f\left(\log_2^{\rho_{max}-\rho_{min}}\right)}, \tag{2}$$

$$n_\theta = 2^{f\left(\log_2 \frac{\theta_{max}-\theta_{min}}{d_\theta}\right)}, \tag{3}$$

where the function $f(\cdot)$ rounds the argument to the nearest integer towards zero.

2.2. Accumulation distribution model of line segment

Before implementing a HT method, firstly the edge pixels in an image should be extracted. Among them, except those belonging to the lines, other pixels act as background clutter or noise. The mesh surface of an accumulator obtained by conventional HT is shown in Fig. 3(a). In the first glance, two peaks can be easily recognized, which correspond to two line segments in the original image, see Fig. 5(b). From the aspect of amplitude, the lowest peak is similar with other parts. The expected peaks still can be identified by our eyes because they are 'isolated'. This motivates us to identify peaks by 'isolating' characteristics.

The accumulation distribution corresponding to an ideal line segment can be described by a butterfly model (Furukawa and Shinagawa, 2003; Leavers and Boyce, 1987), see Fig. 1(a), whose location and orientation are denoted by four parameters: θ_p and ρ_p refer to the peak's position, ϕ_1 and ϕ_2 refer to the upper and lower ridge angles, i.e. indicate the total butterfly's orientation, see Fig. 1(b). Angles ϕ_1 and ϕ_2 are determined by the pixel distributions of the line segment, and vary inside the range of $(-\frac{\pi}{2}, \frac{\pi}{2}]$. Without loss of generality, assuming that $\phi_1 > \phi_2$. The angle between a butterfly's upper and lower ridges, which intersect at the peak, is $\phi_1 - \phi_2$. This quantity varies monotonically with respect to the distance between the two endpoints of the line segment. The proposed algorithm is based on this characteristic.

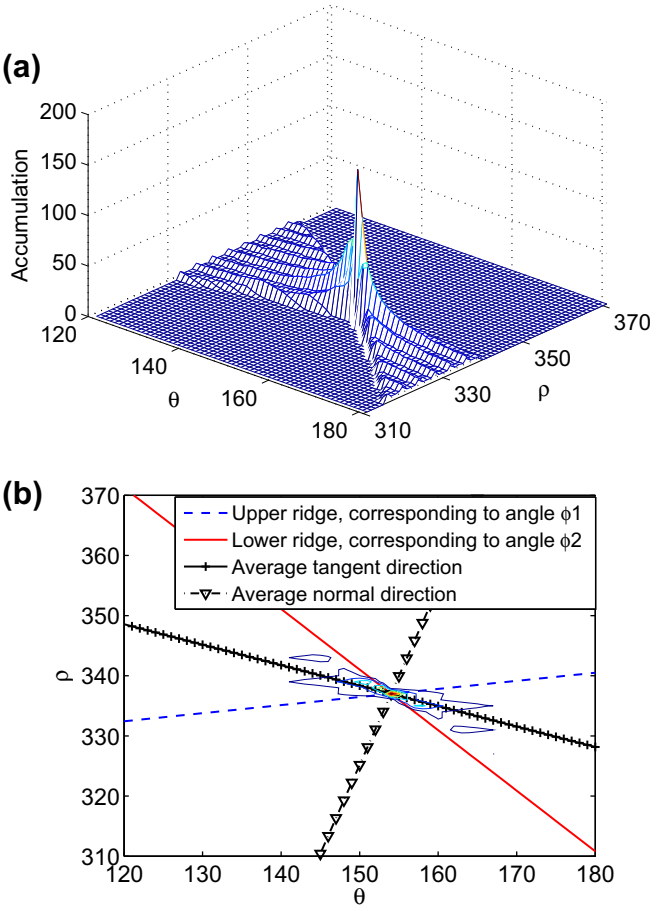

Fig. 1. The mesh surface and contour of an ideal butterfly. (a) The mesh surface of the butterfly. (b) The contour of the butterfly, its upper ridge, lower ridge, average normal direction and average tangent direction at its peak.

2.3. The local operator

To describe the 'isolating' characteristics, the difference of accumulation values between adjacent units is considered. For an ideal butterfly, such differences between its peak and any unit outside the butterfly should be the same, since outside the butterfly, any unit has zero accumulation, see Fig. 1(a). In presence of noise, usually this is not valid. A more conservative result is that from a peak, the accumulation should descend more rapidly along a direction outside the butterfly than a direction inside the butterfly. At a unit, given all curves passing through it, the unit's average normal direction is defined as the average of all the curves' normal directions. Similarly, the unit's average tangent direction is defined too. Obviously, at a butterfly's peak, the average normal and average tangent directions should be mutually perpendicular and located outside and inside the butterfly, respectively, see Fig. 1(b).

Suppose the accumulation value at a butterfly's peak is q, it means that there are q sine curves passing through. Take the lth curve ($1 \leqslant l \leqslant q$) as an instance, whose corresponding image pixel's coordinates are denoted by (x_l, y_l). Given Eq. (1), this curve's slope rate at the peak (θ_p, ρ_p), i.e. the derivative of ρ with respect to θ, can be expressed as:

$$k_l = \frac{d\rho}{d\theta} = -x_l \sin\theta_p + y_l \cos\theta_p \quad l = 1, \ldots, q. \tag{4}$$

According to the definition of a continuous curve's normal and tangent directions, they should be mutually perpendicular, and their slope rates' product should equal to -1. Then the curve's normal direction's slope rate at the peak (θ_p, ρ_p) is:

$$n_l = \frac{1}{x_l \sin\theta_p - y_l \cos\theta_p} \quad l = 1, \ldots, q. \tag{5}$$

In the accumulator, it corresponds to an angle ψ_l relative to the θ axis (anticlockwise):

$$\psi_l = \arctan(n_l) \quad l = 1, \ldots, q. \tag{6}$$

Finally, the angle corresponding to the average normal direction is given by:

$$\bar{\psi} = \frac{1}{q} \sum_{l=1}^{q} \psi_l. \tag{7}$$

For any unit, the angle corresponding to its average normal direction can be calculated by Eqs. (5)–(7). Then the difference of accumulation value between itself and adjacent units are projected to its average normal direction and summed together. Such quantity is adopted to describe how prominent a unit is relative to its neighbors. To keep those quantities, a new matrix R, with the same size of the original accumulator, is built. An element of the original and new matrices is denoted by z_{ij} and r_{ij}, respectively. In the original accumulator, a unit's 8-neighborhood is defined, see Fig. 2. Inside this neighborhood, units are denoted by one letter subscript, e.g. instead of z_{ij}, z_5 is adopted to refer to the central unit. For each neighbor, there is a constant angle β_i depicting its orientation relative to the central unit, i.e. the angle rotated from θ axis to a segment connecting the central unit and this neighbor, anticlockwise. The values from β_1 to β_9 (except β_5) are $\frac{3\pi}{4}$, $\frac{\pi}{2}$, $\frac{\pi}{4}$, π, 0, $\frac{5\pi}{4}$, $\frac{3\pi}{2}$ and $\frac{7\pi}{4}$, respectively. Then an angle γ_i is defined as the deviation between angle β_i and the angle $\bar{\psi}$, calculated by following pseudo codes:

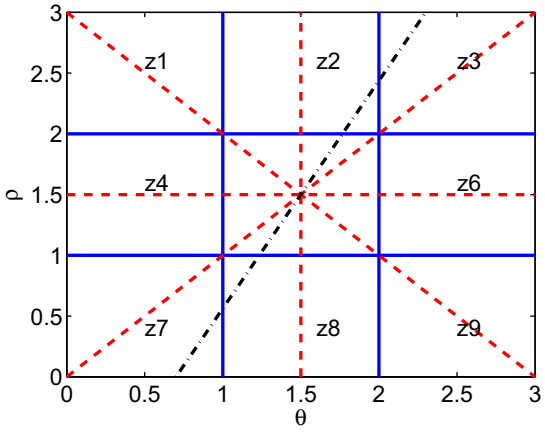

Fig. 2. The definition of an 8-neighborhood in accumulator. The dashed lines represent the neighbors' orientation relative to the central unit, and the dashdot line represents the central unit's average normal direction.

Algorithm 1. The process of computing γ_i

```
γ_i = |β_i − ψ̄|;
if γ_i > 2π then
    γ_i = γ_i − 2π
end if
if γ_i > π then
    γ_i = 2π − γ_i
end if
if γ_i > π/2 then
    γ_i = π − γ_i
end if
```

To calculate the sum, the weight for each neighbor is chosen as $\cos(\gamma_i)$, i.e. to project the difference between the central unit and its neighbors onto the central unit's average normal direction. As a consequence, the unit in matrix R has a value:

$$r_5 = \sum_{i=1}^{9} (z_5 - z_i) \cos\gamma_i. \tag{8}$$

From an expected peak, the drop close to its average normal direction is treated with a larger weight, in contrast, the drop close to its average tangent direction is treated with a smaller weight. Eq. (8) realizes a one to one mapping from matrix Z to matrix R, in other words, acts as an operator. Applying Eq. (8) to all units in the original accumulator, the matrix R will be obtained. Note, for the units on the accumulator's boundaries, some terms in the right side of Eq. (8), will be ignored. The effect of the operator to an accumulator corresponding to Fig. 5(b) is shown in Fig. 3. It can be seen that, after implementing the operator, two peaks become more prominent.

The effect of the operator depends on the accumulation distribution and three phenomena may take place: (1) At peaks caused by lines, the value r is much more than z. The enhancement increases with the butterfly decreasing in angular range (i.e. $\phi_1 - \phi_2$). (2) For some units near the peak, although value z is high also, r becomes smaller or even negative, because the descent from the peak contributes a negative value to the sum. Because of above two effects, a desired peak becomes more 'isolated'. (3) For most peaks caused by noise, which located close to each other, the accumulation distribution satisfies the butterfly mode poorly, the average normal direction acts with less effect. The operator's effect will be demonstrated by statistical analysis on simulation data.

2.4. Simulation on synthesized images

First, the effect is verified with images involving only an ideal line segment. The magnification, i.e. the ratio of the modified accumulation peak to the original accumulation peak is considered. In addition, two windows are defined, the sizes of which are 3×3 and 5×5, respectively, and both centered at the peak. The sum of accumulation inside these windows (except the center) is calculated both before and after implementing the operator. Then the ratio of the transformed sum to the original sum is obtained, see Fig. 4. It can be seen that in spite of the line length, the magnification with respect to the peak is approximately constant, the magnification with respect to the window sums varies with the line length, and always smaller than the peak magnification. In some cases, it is even negative, so the ideal peaks become more prominent.

Then a series of 18 images containing noise are tested. To simulate the effect of edge extraction, noise pixels are not uniformly distributed throughout the image, but in three sub-regions, see Fig. 5(a). In each image, noise pixels appear with a certain probability. There are altogether 18 noise levels, which respectively

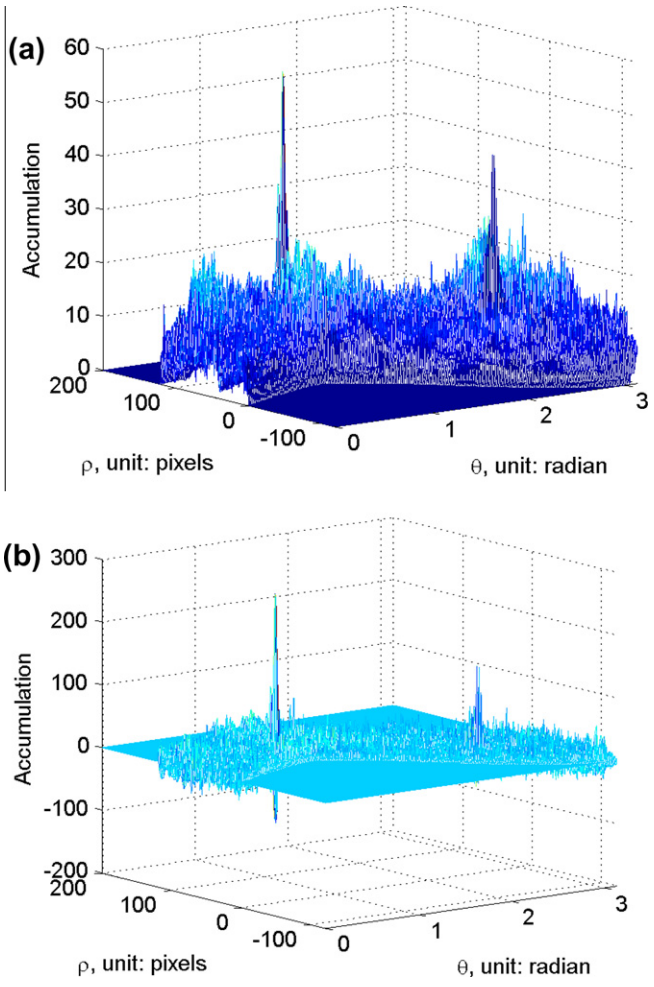

Fig. 3. The effect implementing the operator to an accumulator array. (a) The mesh surface of the accumulator before implementing. (b) The mesh surface of the accumulator after implementing.

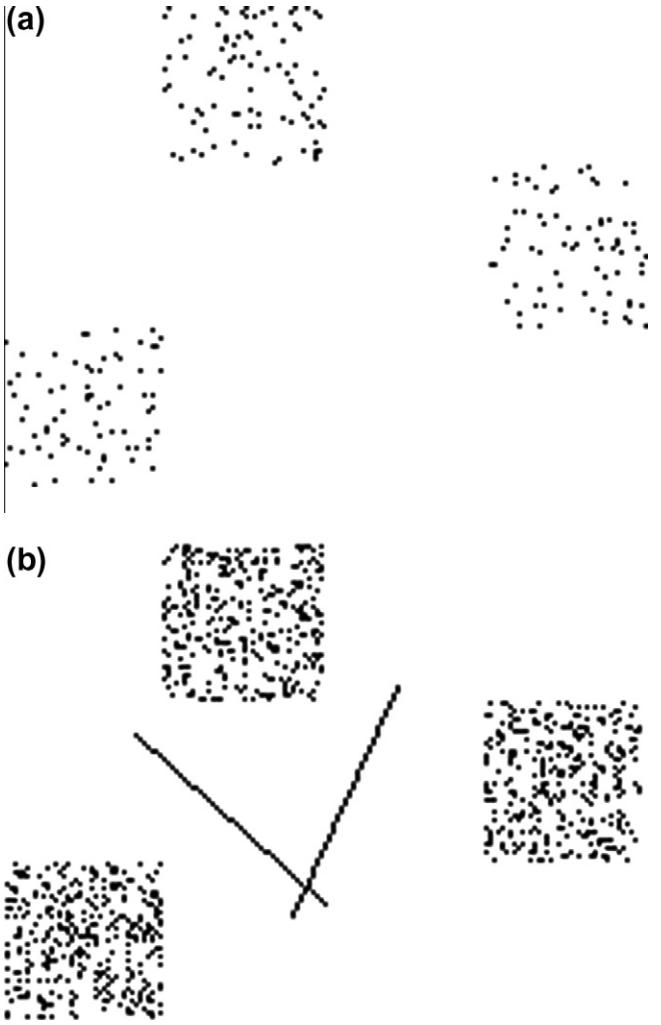

Fig. 5. Two sample images. (a) An image contains only noise pixels, which appear with probability of 3%. (b) An image contains lines and noise pixels, which appear with probability of 18%.

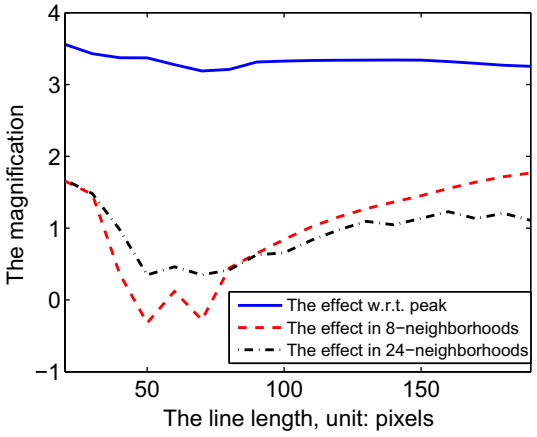

Fig. 4. The accumulation magnification with respect to ideal line segment.

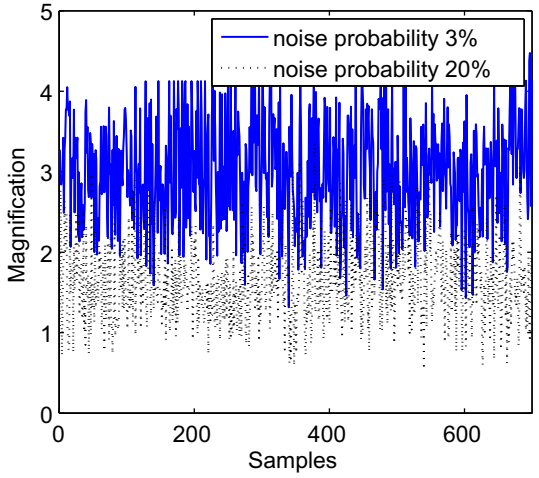

Fig. 6. The magnification effect on two noise levels.

correspond to probabilities vary from 3% to 20% with intervals of one percent. Magnification at all local peaks in the original accumulator are considered. In Fig. 6, two instances are demonstrated. For all the noise levels, the average and variance of the magnification at all peaks are drawn in Fig. 7(a). The average magnification decreases monotonically, and despite the noise level, the variance of the magnification is approximately constant. With a low noise level, the magnification is similar with line segment, since the peaks are located far away from each other. In other words, the

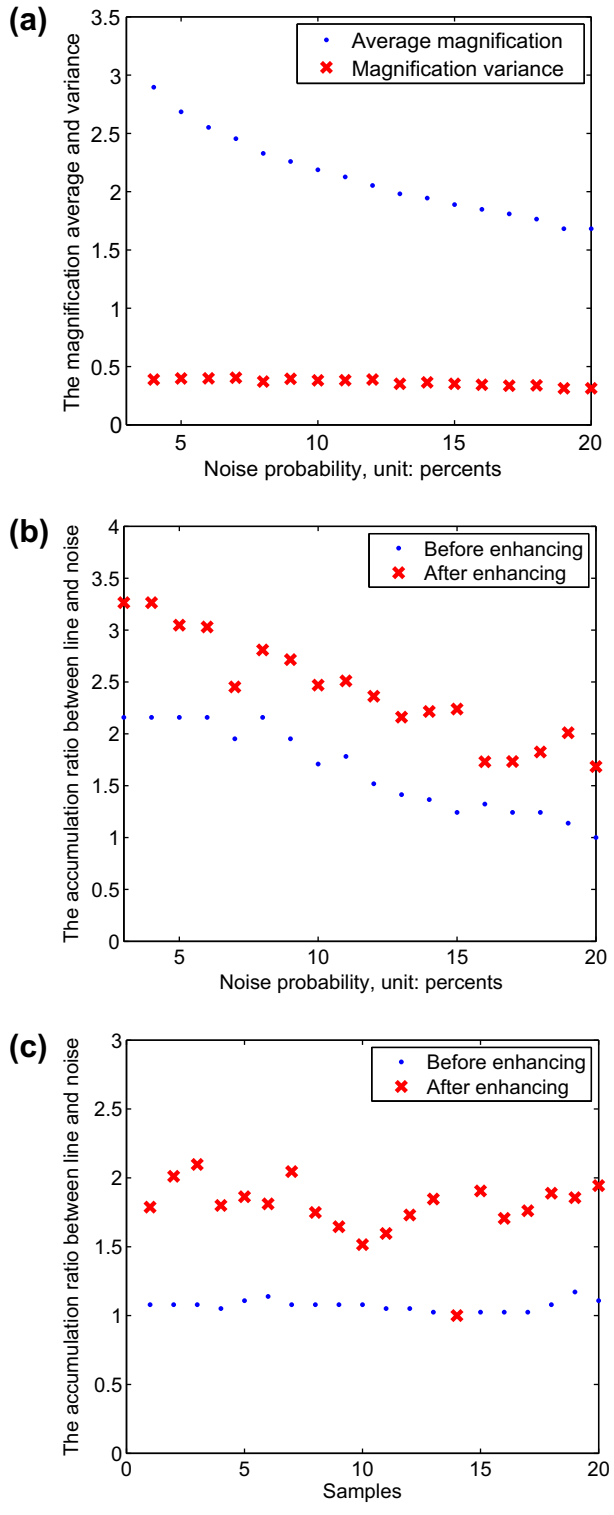

Fig. 7. The effect of the operator on synthesized noisy images. (a) The average magnification and magnification variance with respect to noise. (b) The enhancement about ratio between line and noise. (c) The enhancement about ratio between line and noise at worst situation, probability = 20%.

butterfly pattern is satisfied to some extent. With the noise level increasing, peaks will distribute closer to each other and the butterfly pattern is less satisfied. As a consequence, magnification will decrease. Since the transformed accumulation is the product of the original accumulation and the magnification, the accumulation difference between ideal line segments and noise will be amplified over all noise levels.

Afterwards, two line segments are added to the image series, see Fig. 5(b). The ratio between the accumulations corresponding to the short segment and maximum noise is drawn in Fig. 7(b). Obviously, the ratio decreases with the increasing noise level, both before and after enhancing, the enhancement can be observed as the deviation between the two curves. Special attention is paid to the worst case, i.e. the noise pixel appears with probability of 20%. Before enhancement, the accumulation corresponding to the short line segment almost equals to the maximum accumulation caused by noise. 20 sample images are generated under this assumption, and the proposed operator is applied to each image, see Fig. 7(c). It can be found that, after enhancement, although for most images the ratio between line segment and maximum noise fluctuates from 1.5 to 2.1, for some case (sample No.14), the operator does not work. Such situation can be considered as the critical point of the proposed method's effectiveness. This is easy to understand, since in such situation, the number of noise pixels is equal to or greater than the expected line length.

3. Peak location

Global threshold is adopted to locate accumulation peaks. In real images, the ratio between pixel numbers of a line segment and background clutter is influenced by some aspects, e.g. from where the image was taken, or whether part of the line segment is overlapped by other things, etc. To achieve better robustness, it is necessary to find a way to determine the threshold valid for different images.

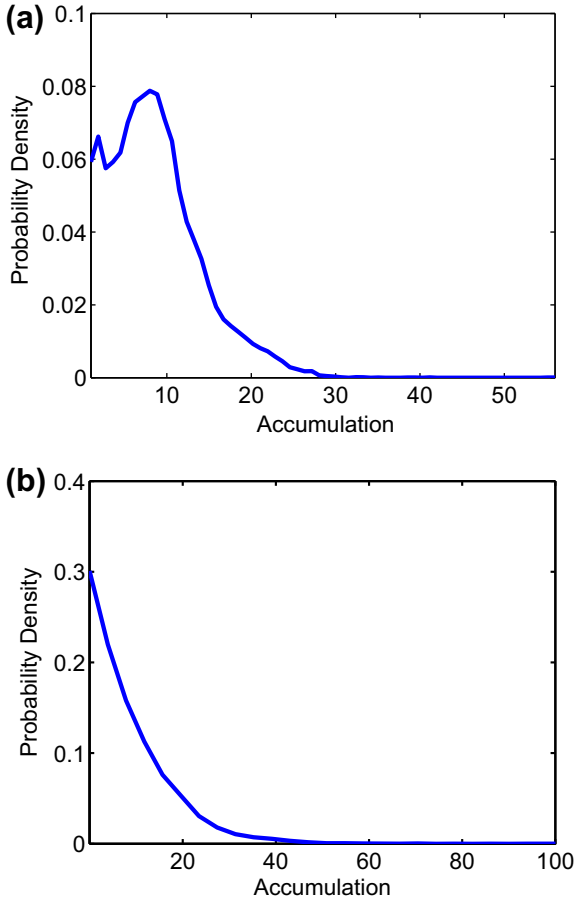

Fig. 8. The histogram of accumulator, the noise level in the original image is 15%. (a) The histogram before enhancing. (b) The histogram formed by all positive values after enhancing.

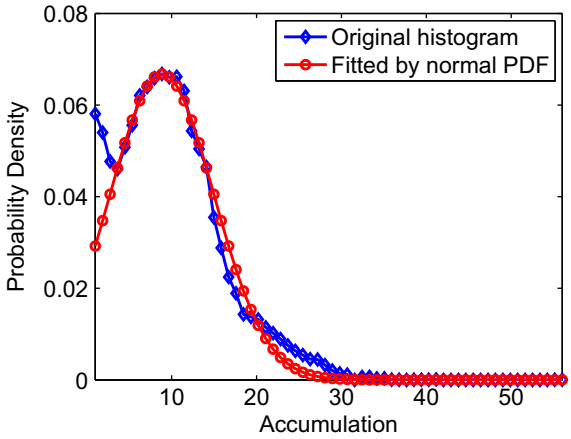

Fig. 9. The fitting effect by a normal PDF.

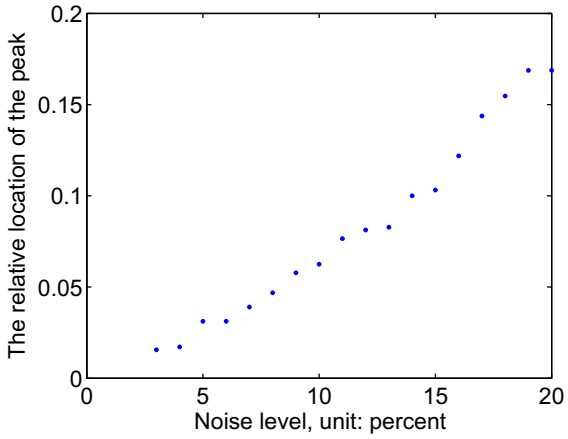

Fig. 10. The mapping between noise level and histogram peak location.

The accumulation histograms before and after enhancing for a sample images are drawn in Fig. 8. After enhancing, only positive values are considered to form the histogram, since negative part is useless to determine the threshold, because a peak can not occur with a negative value. Some phenomena can be observed: (1) Before enhancing, the histogram looks like a normal Probability Density Function (PDF), after enhancing, it looks like a negative exponential PDF. (2) After enhancing, the difference between the histogram shapes is reduced. (3) Before enhancing, when there is more image noise, the more rightwards the maximum value is located and the wider the peak. (4) After enhancing, the 'flat' area, corresponding to high accumulation value, becomes wider. This coincides with the analysis of the simulation result.

The threshold can be determined by analyzing the histogram shape. Intuitively, the boundary between the 'steep' and 'flat' parts in the original histogram could act as the threshold. Since the original histogram looks like a normal PDF, Gaussian distribution function (Amari and Nagaoka, 2000) is adopted for fitting. μ is

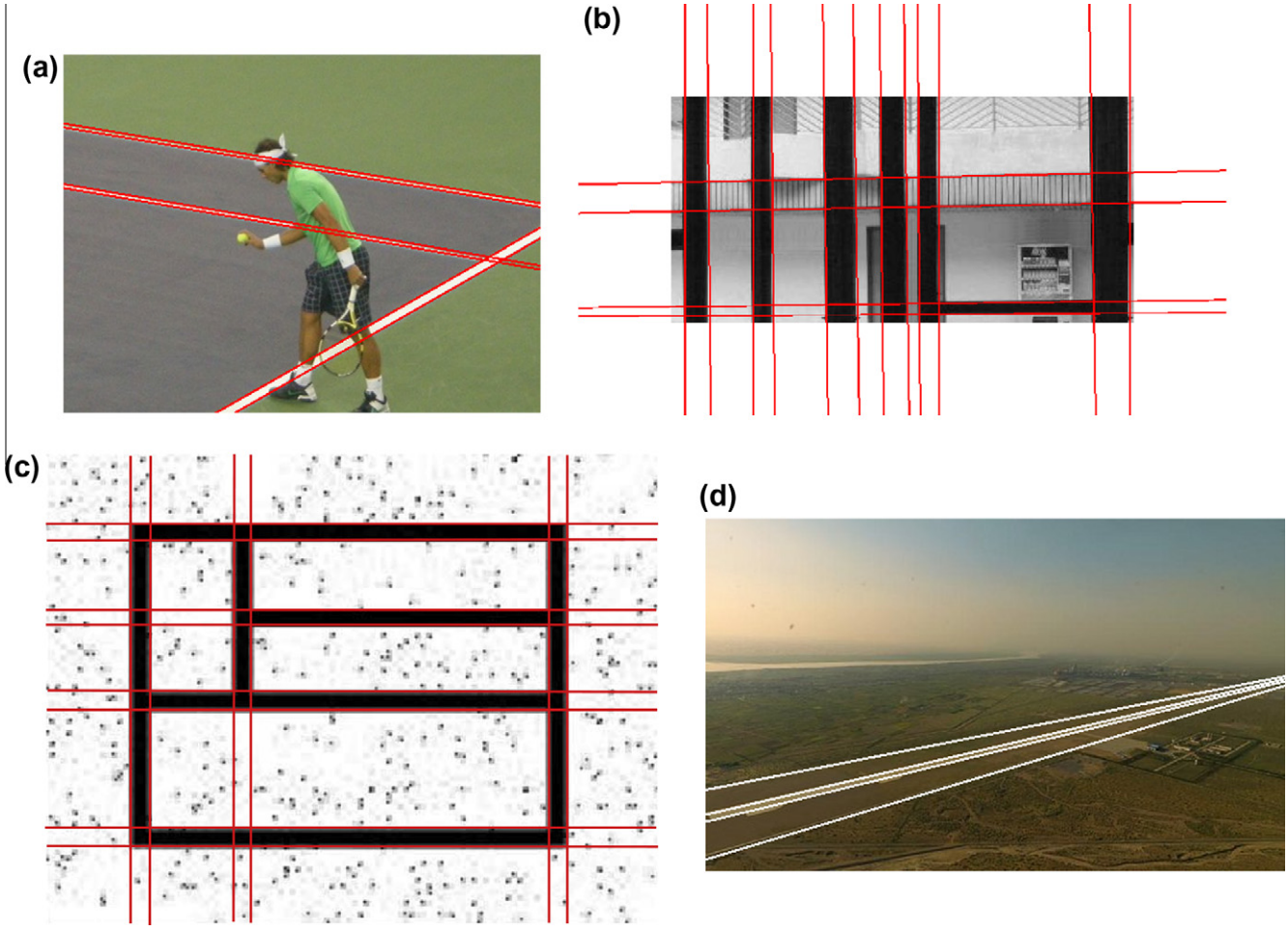

Fig. 11. Experiments results of the proposed method.

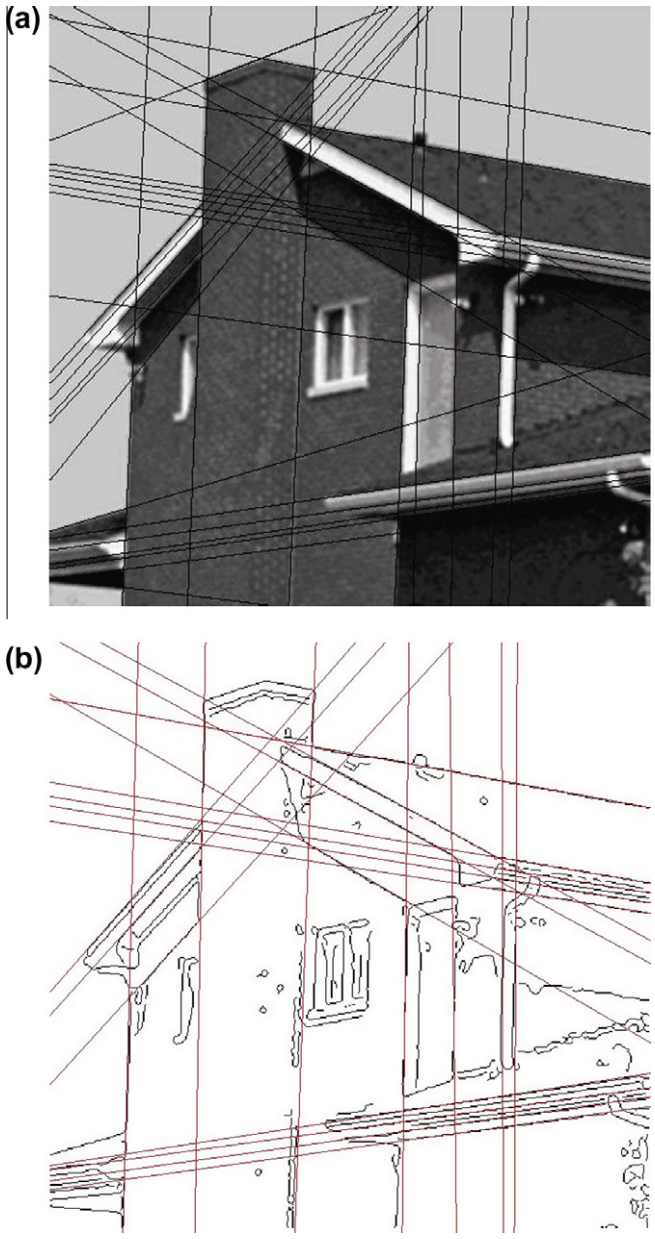

Fig. 12. The ground truth lines and extracted result of a sample image. (a) The original image and expected line segments chosen manually. (b) The extracted edges by Canny operator and the detected lines by the proposed method.

chosen as the accumulation corresponding to the maximum probability density, $\mu + \sigma$ corresponding to the maximum probability density times 0.6065. A fitting sample is shown in Fig. 9, where $\mu + 3\sigma$ is quite close to the boundary between the 'steep' and 'flat' parts. The effect of adopting this threshold directly on many images is poor, either false-positive or false-negative appears often, especially with strong noise. To realize the benefit of the operator, a threshold can be determined in the histogram of the enhanced accumulator. Given an accumulation value in the original histogram, there should be a corresponding value in the enhanced histogram. In Fig. 7(a), it can be seen that the magnification about noise varies with respect to the noise level, so choosing a suitable magnification will be helpful to achieve a better solution. Considering the 3rd observation with respect to histogram, the mapping between maximum probability density's location and the noise level is drawn in Fig. 10.

Some intermediate variables are defined for clarity of presentation. x_p is the accumulation corresponding to the maximum probability density in the original histogram, x_1 can be any accumulation in the original histogram, in this case it corresponds to $\mu + 3\sigma$, n is the image noise level, m is the magnification factor for noise depending on the noise level, p is the ratio between magnification for line segment and noise, and x_2 is the accumulation (threshold) in the enhanced histogram. Given x_p and x_1, the task is determining x_2. n, m and p act as intermediate variables. The relationship between variables can be expressed as:

$$n = f(x_p), \tag{9}$$

$$m = g(n), \tag{10}$$

$$x_2 = p \cdot m \cdot x_1. \tag{11}$$

The functions $f(\cdot)$ and $g(\cdot)$ can be fitted from Figs. 10 and 7(a), respectively. To treat the worst cases, the magnification is increased by a variance, which is a constant, see Fig. 7(a). p is chosen as 1.5, the minimum valid value in Fig. 7(c). For all the sample images, the obtained x_2 is located inside the 'flat' part of the enhanced histogram.

Note, in above description, n represents the noise level in Fig. 5(a), i.e. the noise pixels are distributed only in three sub-regions. Simulation result shows that there are similar mappings between peak location in the histogram and noise level, while noise distributes in different ways. Here, n acts as a general purpose variable reflecting noise level.

It is also possible to directly fit the enhanced histogram by a negative exponential function, and then determine the threshold by choosing a suitable probability density. The major difficulty is that as already mentioned the flat part of the enhanced histogram is quite wide. It's easy to generate either a false-positive or false-negative by an inappropriate threshold. We think the major reason is the information with respect to the image noise is not considered. In Eqs. (9)–(11), information about noise is implicitly involved, based on such information, the threshold is obtained. As a consequence, better performance is achieved.

4. The experimental results

The effect of the proposed method is verified with real images, five samples are shown in Figs. 11 and 12. The Canny operator is adopted to extract boundaries. In sub-figures Fig. 11(a–c), all ground truth lines are drawn in red, while in Fig. 11(d), ground truth lines are drawn in white. In Fig. 12, the ground truth lines determined by us manually are marked in the original image. In contrast, the detection results are marked in the extracted boundaries.

Some other methods were also tested, which are randomized HT (running for ten times, then the average results were taken), probabilistic HT (running for ten times, then the average results were taken), sampling HT (with window of size 5×5), PCA method, Ridgelet method and the butterfly based method (BF for short)

Table 1
The number of detected lines in sample images.

Figure	Methods						
	RHT	PHT	SHT	PCA	Ridgelet	BF	Ours
Fig. 11(a)	3.5	4.2	4	3	4	4	6
Fig. 11(b)	8.3	7.5	14	7	11	19	14
Fig. 11(c)	10.3	12.2	13	8	9	14	16
Fig. 11(d)	2.8	2.9	3	4	3	7	4
Fig. 12	15.3	18.8	19	24	19	39	22

Table 2
The number of false-positive (FP) and false-negative (FN) caused by different methods.

Figure	RHT		PHT		SHT		PCA		Ridgelet		BF		Ours	
	FP	FN	FP	FN	FP	FN	FP	FN	FP	FN	FP	FN	FP	FN
Fig. 11(a)	0	2.5	0	1.8	0	2	0	0	0	2	0	2	0	0
Fig. 11(b)	0	5.7	0	6.5	0	0	0	0	0	3	5	0	0	0
Fig. 11(c)	0	5.7	0	3.8	0	3	0	0	0	5	0	2	0	0
Fig. 11(d)	0	1.2	0	1.1	0	1	0	0	0	1	3	0	0	0
Fig. 12	0	16.7	0	13.2	0	13	0	8	0	13	8	0	0	10

in Furukawa and Shinagawa (2003). The number of detected lines is listed in Table 1, the number of false-positives and false-negatives are listed in Table 2. The proposed method gives a good performance on detection correctness. For the PCA method, essentially, it detects the center line of line strips. Except Fig. 11(d) and Fig. 12, the number extracted by PCA method is half of our results, since the proposed method extract both boundaries of a line strip, the PCA's result is still recognized as correct.

In Fig. 12, there are 32 ground truth lines, for our method, the number of false-negatives is 10, i.e. 10 lines are missed, mainly, it is due to two reasons. First, some short line segments are ignored, e.g. the chimney's edges, second, while some lines are close to each other, e.g. at the eaves close to the right boundary of the image, some of them is missed because their corresponding peaks are too close to be distinguished from each other. This is a task to be solved in future work.

For Fig. 12, either PCA or BF method gives better performance. To achieve this effect, much time and effort is consumed tuning the parameters, especially when there is more than one parameter. For our method, no parameters are needed to be tuned, that is its major advantage compared to most existing methods.

The radial and angular accuracy of the extracted lines are also compared, as there is no correct answer, such work is done manually and all the methods give similar accuracy.

5. The conclusion

In this article, an improved Hough transform method to detect line segments is proposed, which makes two major contributions: a local operator in the parameter space is defined to enhance the difference between accumulation peaks caused by real line segments and noise. Global threshold in the enhanced accumulation array is obtained by analyzing the shape of original accumulator histogram and the enhancing effect for line segments and noise.

The experimental results show that the proposed method is quite effective and robust to extract lines in spite of noise and partial disconnection without any prior knowledge.

Compared to other methods, there is no parameter tuning needed to adapt to different images. A time-consuming task is avoided and the method can be implemented more autonomously and the effect is less influenced.

Acknowledgment

The work of this article is supported by Natural Science Foundation of China, under contract number 60405008. The authors thank the anonymous reviewers and the editors for their many helpful suggestions. The authors would also like to thank Dr.Thierry Garaix from Politecnico di Torino, Italy, for his constructive suggestions and kind help.

References

Aghajan, H., Kailath, T., 1995. Subspace-based line detection. US Patent 5,418,892.
Amari, S., Nagaoka, H., 2000. Methods of Information Geometry. Oxford University Press, Oxford.
Atiquzzaman, M., Akhtar, M., 1995. A robust hough transform technique for complete line segment description. Real-Time Imaging 1, 419–426.
Bonci, A., Leo, T., Longhi, S., 2005. A Bayesian approach to the Hough transform for line detection. IEEE Trans. Systems Man Cybernet., Part A: Syst. Humans 35 (6), 945–955.
Cha, J., Cofer, R., Kozaitis, S., 2006. Extended hough transform for linear feature detection. Pattern Recognit. 39, 1034–1043.
Chien, J., Li, C., 1997. Wavelet-based line detection in gray-scale images. In: 1997 IEEE Internat. Conf. on Systems Man Cybernet., 1997. Computational Cybernetics and Simulation, vol. 4.
Duda, R., Hart, P., 1972. Use of hough transformation to detect lines and curves in pictures. Graphics Image Process. 15, 11–15.
Furukawa, Y., Shinagawa, Y., 2003. Accurate and robust line segment extraction by analyzing distribution around peaks in hough space. Computer Vision and Image Understanding 92, 1–25.
Hou, B., Liu, F., Jiao, L., 2003. Linear feature detection based on ridgelet. Sci. China (Series E) 46, 141–152.
Hough, P., 1962. Methods and means for recognizing complex patterns. Tech. Rep. 3069654, US Patent.
Kiryati, N., Bruckstein, A., 2000. Heteroscedastic hough transform (htht): an efficient method for robust line fitting in the 'errors in the variables' problem. Computer Vision and Image Understanding 78, 69–83.
Kiryati, N., Elar, Y., Bruckstein, A., 1991. A probabilistic hough transform. Pattern Recognit. 24, 303–316.
Leavers, V., Boyce, J., 1987. The radon transform and its application to shape parametrization in machine vision. Image Vision Comput. 5, 161–166.
Li, Z., Liu, Y., Hayward, R., Zhang, J., Cai, J., 2008. Knowledge-based power line detection for UAV surveillance and inspection systems. In: Image Vision Comput. New Zealand, 2008. IVCNZ 2008. 23rd Internat. Conf., pp. 1–6.
Liu, Z., Chiu, K., Xu, L., 2003. Strip line detection and thinning by RPCL-based local PCA. Pattern Recognition Lett. 24 (14), 2335–2344.
Lu, G., Xu, H., Li, Y., 2005. Line detection based on chain code detection. In: IEEE Internat. Conf. on Vehicular Electronics and Safety, 2005. pp. 98–103.
Matas, J., Galambos, C., Kittler, J., 2000. Robust detection of lines using the progressive probabilistic hough transform. Computer Vision and Image Understanding 78, 119–137.
Palmer, P., Kittler, J., Petrou, M., 1997. An optimizing line finder using a hough transform algorithm. Computer Vision and Image Understanding 67, 1–23.
Ser, P., Siu, W., 1992. Sampling hough algorithm for the detection of lines and curves. In: IEEE Internat. Symp. on Circuits Syst. pp. 2497–2500.
Shaked, D., Yaron, O., Kiryati, N., 1996. Deriving stopping rules for the probabilistic hough transform by sequential. Computer Vision and Image Understanding 63, 512–526.
Soffer, M., Kiryati, N., 1998. Guaranteed convergence of the hough transform. Computer Vision and Image Understanding 69, 113–134.
Song, J., Lyu, M., 2005. A hough transform based line recognition method utilizing both parameter space and image space. Pattern Recognit. 38, 539–552.
Xu, L., Oja, E., 1993. Randomized hough transform (rht): basic mechanisms, algorithms and computational complexities. CVGIP: Image Understand 57, 134–154.
Xu, L., Oja, E., Kultanen, P., 1990. A new curve detection method: randomized hough transform (rht). Pattern Recognition Lett. 11, 331–338.
Yang, M., Lee, J., Lien, C., Huang, C., 1997. Hough transform modified by line connectivity and line thickness. IEEE Trans. Pattern Anal. Machine Intell. 19, 905–910.
Zheng, Y., Li, H., Doermann, D., 2005. A parallel-line detection algorithm based on HMM decoding. IEEE Trans. Pattern Anal. Machine Intell., 777–792.